ACS chemical biology

This article is made available via the ACS COVID-19 subset for unrestricted RESEARCH re-use and analyses in any form or by any means with acknowledgement of the original source. These permissions are granted for the duration of the World Health Organization (WHO) declaration of COVID-19 as a global pandemic.

ACS CORONAVIRUS RESEARCH LICENSE

pubs.acs.org/acschemicalbiology

Articles

A Clinical-Stage Cysteine Protease Inhibitor blocks SARS-CoV-2 Infection of Human and Monkey Cells

Drake M. Mellott, Chien-Te Tseng, Aleksandra Drelich, Pavla Fajtová, Bala C. Chenna, Demetrios H. Kostomiris, Jason Hsu, Jiyun Zhu, Zane W. Taylor, Klaudia I. Kocurek, Vivian Tat, Ardala Katzfuss, Linfeng Li, Miriam A. Giardini, Danielle Skinner, Ken Hirata, Michael C. Yoon, Sungjun Beck, Aaron F. Carlin, Alex E. Clark, Laura Beretta, Daniel Maneval, Vivian Hook, Felix Frueh, Brett L. Hurst, Hong Wang, Frank M. Raushel, Anthony J. O'Donoghue, Jair Lage de Siqueira-Neto, Thomas D. Meek,[$] and James H. McKerrow*,[$]

Cite This: https://doi.org/10.1021/acschembio.0c00875

Read Online

ACCESS | Metrics & More | Article Recommendations | Supporting Information

ABSTRACT: Host-cell cysteine proteases play an essential role in the processing of the viral spike protein of SARS coronaviruses. K777, an irreversible, covalent inactivator of cysteine proteases that has recently completed phase 1 clinical trials, reduced SARS-CoV-2 viral infectivity in several host cells: Vero E6 (EC_{50}< 74 nM), HeLa/ACE2 (4 nM), Caco-2 (EC_{90} = 4.3 μM), and A549/ACE2 (<80 nM). Infectivity of Calu-3 cells depended on the cell line assayed. If Calu-3/2B4 was used, EC_{50} was 7 nM, but in the ATCC Calu-3 cell line without ACE2 enrichment, EC_{50} was >10 μM. There was no toxicity to any of the host cell lines at 10−100 μM K777 concentration. Kinetic analysis confirmed that K777 was a potent inhibitor of human cathepsin L, whereas no inhibition of the SARS-CoV-2 cysteine proteases (papain-like and 3CL-like protease) was observed. Treatment of Vero E6 cells with a propargyl derivative of K777 as an activity-based probe identified human cathepsin B and cathepsin L as the intracellular targets of this molecule in both infected and uninfected Vero E6 cells. However, cleavage of the SARS-CoV-2 spike protein was only carried out by cathepsin L. This cleavage was blocked by K777 and occurred in the S1 domain of the SARS-CoV-2 spike protein, a different site from that previously observed for the SARS-CoV-1 spike protein. These data support the hypothesis that the antiviral activity of K777 is mediated through inhibition of the activity of host cathepsin L and subsequent loss of cathepsin L-mediated viral spike protein processing.

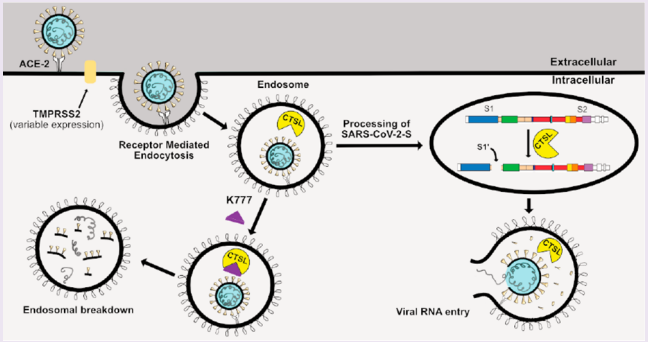

INTRODUCTION

The COVID-19 outbreak of 2019[1,2] has led to a global health crisis of a magnitude not seen since the influenza pandemic of 1918. By March 2021, more than 118 million people have been infected worldwide, including more than 29 million in the U.S.[3,4] Accordingly, there is an urgent need for the rapid identification of therapies that limit the pathology caused by SARS-CoV-2 for the management of COVID-19.[5,6]

The severe acute respiratory syndrome (SARS) and Middle East respiratory syndrome (MERS) outbreaks of 2003 and 2012,[7,8] caused by betacoronaviruses highly related to SARS-CoV-2, provided important clues to the mechanism of viral infection of host cells. Two virally encoded cysteine proteases, 3CL protease (3CLpro)[9] and a papain-like protease (PLpro),[10] are essential to coronaviral maturation. In addition, the trimeric coronaviral spike glycoprotein of SARS-CoV-2 (76% sequence identity to SARS-CoV-1 spike protein[11]) is involved in the fusion of the viral envelope with mammalian cell membranes, followed by the release of the genomic viral RNA and the nucleocapsid complex into the host cell[12,13] Studies of the SARS-CoV-1 spike protein reveal that it adheres to the extracellular domain of the angiotensin converting enzyme-2 (ACE2) receptor in susceptible human cells.[11,14,15] In SARS-CoV-2, the receptor binding domain of the spike protein subunit S1 binds to the ACE2 receptor, and subunit S2 is involved in the viral cell membrane fusion to facilitate viral entry.[16,17] Prior to cellular entry, the spike protein requires processing by host cell proteases for activation.[15,16,18,19] In particular, the transmembrane protease serine-2 (TMPRSS-2), the cysteine

Received: November 9, 2020
Accepted: March 18, 2021

© XXXX American Chemical Society

protease cathepsin L (CTSL), and furin-like proteases have been proposed to play a role in preparing SARS-CoV-2 to enter cells by either endocytosis or traversing the cellular membrane.[16,17,19−21]

The proposed roles of host proteases in viral infection have stimulated studies to explore whether serine and/or cysteine protease inhibitors reduce coronaviral entry. Inhibitors of TMPRSS-2, such as camostat, reduced infectivity in selected human cell lines.[16] Broad spectrum cysteine protease inhibitors, such as E-64d, also inhibited coronaviral entry in certain cell types.[16,20,21] Riva *et al.* also reported in a drug repositioning screen that several cathepsin inhibitors have the ability to block SARS-CoV-2 entry into cells at submicromolar concentrations.[22]

K777 (also known as K11777, S-001, SLV213, and 4-methyl-N-((S)-1-oxo-3-phenyl-1-(((S)-1-phenyl-5-(phenylsulfonyl)-pentan-3-yl)amino)propan-2-yl)piperazine-1-carboxamide) is a highly potent, irreversible, covalent inhibitor of mammalian cathepsin L and other cysteine proteases of clan CA (Figure 1).[23,24] K777 was originally developed as an inhibitor of

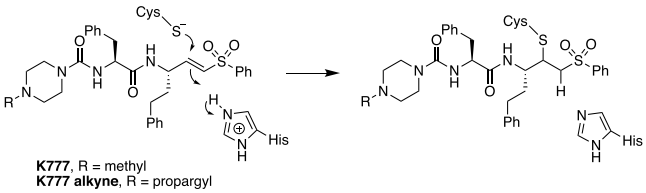

Figure 1. Structure of K777 and its alkynyl analog.[25] Chemical mechanism of irreversible covalent inactivation of clan CA cysteine proteases.

cathepsin S[23] but later showed promise as an antiparasitic agent.[24−30] In 2015, Zhou and colleagues reported that K777 blocked the entry of pseudovirus forms of SARS-CoV-1 and MERS into Vero E6 or HEK293 cells, likely due to inactivation of cathepsin L (CTSL) on cell surfaces and/or within endosomes.[19] These results suggested that K777 might also be a potential therapeutic agent for the treatment of COVID-19. Here, we show that K777 blocks CTSL-mediated processing of the spike protein, and blocks infection of SARS-CoV-2 in several mammalian cell lines. In addition, Selva Therapeutics has an open Investigational New Drug (IND) application with the U.S. FDA for K777 as a possible therapeutic treatment of COVD-19 infection (communicated by Selva Therapeutics, Del Mar, CA).

RESULTS AND DISCUSSION

K777 Blocks SARS-CoV-2 Infectivity of Host Cells. Table 1 shows EC_{50} (or EC_{90} for Caco-2 cells) values for inhibition of viral invasion of host cells by K777, usually assessed by reduction of the cytopathic effect (CPE). The EC_{50} is defined as the concentration of K777 that reduces viral infectivity by 50%, whereas the EC_{90} reports on a 90% reduction. For Caco-2 cells, virus yield reduction was used, as CPE was not observed. EC_{50} values ranged from 4 nM for HeLa/ACE2 cells to 7 nM for Calu-3/2B4 cells, ≥70 nM for Vero cells, <80 nM for A549/ACE2 cells, and >10 μM for Calu-3(ATCC) cells. Caco-2 cells showed an EC_{90} of 4.3 μM. No host cell toxicity was seen for any cell line at inhibitor concentrations of 10−100 μM. The differences between Calu-3 and Calu-3 2B4 cells are especially notable and likely are the result of enrichment of the ACE2 receptor in the latter cells.[31] Figures 2 and S11 show examples of dilution curves used to calculate EC_{50} values. For comparison, the EC_{90} of the known antiviral remdesivir is 0.10 μM in the Caco-2 assay (Figure S11).

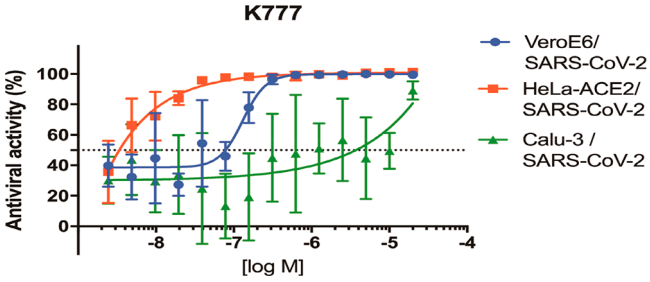

Figure 2. Dose dilution curves for K777 effects on virus infection of three cell lines.

Analysis of K777 versus SARS-CoV-2 and Clan CA Cysteine Proteases. In assays carried out at both UC San Diego and Texas A&M University, there was no inhibition of either the PL and 3CL proteases of SARS-CoV-2 (25−100 nM enzyme concentration) at up to 100 μM K777 (Table 2; Figure S5). Conversely, K777 exhibited potent activity against human cathepsin L, where the second-order rate constant of

Table 1. Anti-Coronaviral Activity of K777 in Infected Primate and Human Cells

cell line	cell type	coronavirus	laboratory	inhibition of viral infectivity EC_{50} (μM)	cytotoxicity to host cells CC_{50} (μM)
Vero E6	African Green monkey/kidney epithelial	SARS-CoV-1[a]	UTMB	2.5	>10
Vero E6		MERS[a]	UTMB	0.62	>10
Vero E6		SARS-CoV-2[a]	UTMB	0.62	>10
Vero E6		SARS-CoV-2	USU	<0.1	>10
Vero E6		SARS-CoV-2	UCSD	0.07	>10
Caco-2	human colon carcinoma	SARS-CoV-2	USU	4.3[c]	>10
A549/ACE-2	human lung carcinoma expressing ACE-2 receptor	SARS-CoV-1[b]	UTMB	0.08	>10
A549/ACE-2		MERS[b]	UTMB	0.08	>10
A549/ACE-2		SARS-CoV-2[b]	UTMB	<0.08	>10
HeLa/ACE-2	human cancer cells expressing ACE-2 receptor	SARS-CoV-2	UCSD	0.004	>10
Calu-3/2B4	human lung adenocarcinoma	SARS-CoV-2[b]	UTMB	0.007	>10
Calu-3	human lung adenocarcinoma	SARS-CoV-2	UCSD	>10	>20

[a]Infected with 100 viral particles/sample. [b]Infected with 500 viral particles/sample. [c]Value is EC_{90}. Laboratories designated are UTMB, University of Texas, Medical Branch; USU, Utah State University; UC SD, University of California, San Diego.

https://doi.org/10.1021/acschembio.0c00875
ACS Chem. Biol. XXXX, XXX, XXX−XXX

Table 2. Inactivation or Inhibition of Mammalian and CoV-2 Cysteine Proteases[a]

enzyme	K_I (nM)	K_{inact} (s^{-1})	K_{inact}/K_I (M^{-1} s^{-1})
human cathepsin L	50 ± 20	0.013 ± 0.002	$(3 \pm 1) \times 10^6$
human cathepsin K	400 ± 100	0.022 ± 0.004	$(6 \pm 2) \times 10^4$
human cathepsin B	3000 ± 1000	0.026 ± 0.007	$(9 \pm 4) \times 10^3$
human cathepsin C	>100,000	ND	$(1.2 \pm 0.4) \times 10^1$[b]
human cathepsin S	2.0 ± 0.1[c]	ND	ND
SARS-CoV-2 3 CL pro	>100,000	ND	ND
SARS-CoV-2 PL	>100,000	ND	ND

[a]pH = 5.5 for cathepsins and pH 7.0 for CoV-2 proteases; ND, not determinable. [b]Value approximated from slope of k_{obs} vs inhibitor. [c]Value represents overall dissociation constant.

inactivation, k_{inact}/K_I, was found to be 50-fold and 333-fold greater than cathepsin K and cathepsin B, respectively (Table 2, Figures S1−S4). K777 formed apparent irreversible covalent adducts with these enzymes (Figure S3) but exhibited weak, slowly reversible, inhibition of cathepsin C and potent but rapidly reversible inhibition of cathepsin S (Figure S4).

Activity-Based Protein Profiling of K777 Protein Targets in Vero E6 Cells. We prepared a K777 analog, K777 alkyne[25] (Figure 1), to elucidate the cellular target(s) of K777. This activity-based protein probe has been used previously to identify the cathepsin-L-like and cathepsin-B-like proteases found in the parasitic protozoan, *Trypanosoma brucei*.[25] The K777 alkyne probe facilitates copper-mediated cycloaddition chemistry between an azide and alkyne both to enrich target proteins for mass spectrometry analysis and for visualization of target proteins via in-gel fluorescence. In both virally and nonvirally infected Vero E6 cells, the protein(s) bound to the K777-Cy7 conjugate had a molecular weight of approximately 25 kDa (Figure 3A), a molecular weight that could correspond to either cathepsin B (mature form: 25 kDa) or cathepsin L (mature form: 24.2 kDa). To confirm that the specificity of the K777 alkyne was analogous to that of K777, cells were also preincubated with 1 μM K777 prior to treatment with the K777 alkyne probe. This resulted in >80% blockage of the 25-kDa target protein signal in both virally and nonvirally infected cells (Figure 3B). As the other minor protein bands visualized were unchanged upon K777 pretreatment, it is concluded that these proteins are not targets of K777.

When comparing the intensity of the 25-kDa band in SARS-CoV-2-infected cells to that of its uninfected counterpart there was nearly a 5-fold decrease in intensity (Figure 3A,B). Reduction of the signal for this band in the virally infected samples may be due to either a reduction of total protein or differential expression of the target(s) of the K777 alkyne. To investigate this, we immunoblotted the housekeeping protein human β-actin to compare its relative amounts in both sets of samples. Upon quantifying the difference in β-actin content between the SARS-CoV-2-infected and uninfected cells, we measured a 5.7-fold decrease in total β-actin signal in the Vero E6 SARS-CoV-2 infected samples (Figures 3C,D and S7). Comparison of the relative intensities of the β-actin band versus the 25-kDa enriched protein for both SARS-CoV-2 infected and uninfected cells approximated a 1:1 ratio (Figure 3E). These results suggested that coronaviral infection of Vero E6 causes a global reduction in protein expression, in agreement with recent reports that nonstructural protein-1 of SARS-CoV-2 suppresses protein translation in infected cells.[32]

Identification of Cathepsin B and L as K777 Targets by Affinity Enrichment and Proteomic Analysis. To identify the molecular target(s) of the K777 alkyne, affinity enrichment and proteomic analysis of treated Vero E6 cell lysates was carried out with variable concentrations of the K777 alkyne (0−10 μM; Figure S8A). A total of 117 proteins at a false discovery rate of 1% were identified, of which 65 were present in the K777 alkyne-treated samples, but not the untreated control (Figure S8B). Proteins of the highest abundance in the treated group (5 and 10 μM samples), as determined by MaxQuant LFQ analysis,[33] were cathepsin B (CTSB) and cathepsin L (CTSL).

Cathepsin L but Not Cathepsin B Catalyzes Cleavage of the SARS-CoV-2 Spike Protein. Having identified CTSB and CTSL as putative targets of K777 in cells, we sought to elucidate the ability of these proteins to process the SARS-CoV-1 and SARS-CoV-2 spike proteins *in vitro*. We determined that both proteases could process the SARS-CoV-1 spike protein, but only human CTSL could process the SARS-CoV-2 spike protein

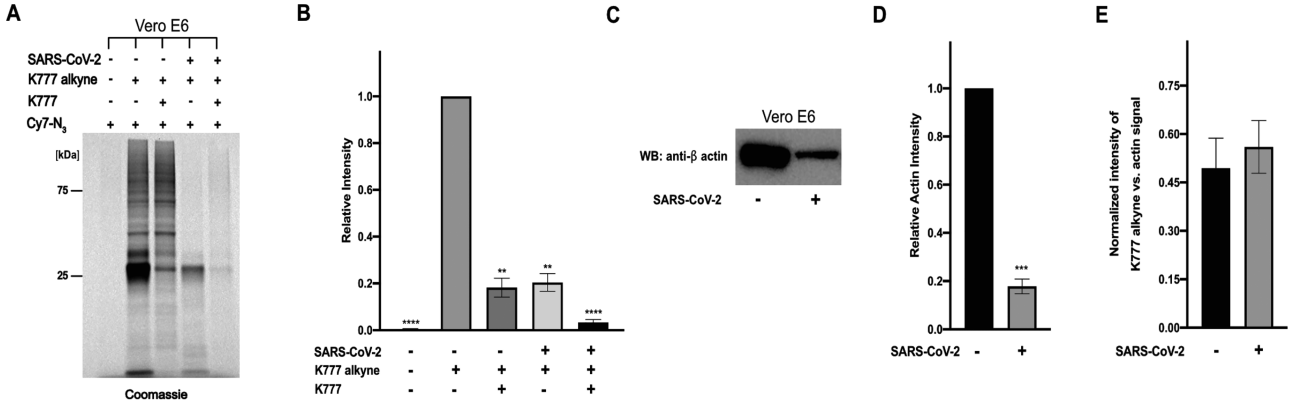

Figure 3. K777 alkyne specifically targets a nonviral protein in SARS-CoV-2 infected and uninfected Vero E6 cells. (A) Cy7 azide labeled proteins (SARS-CoV-2 infected and uninfected) at 1 μM K777 alkyne are blocked by pretreatment with 1 μM K777. (B) Densitometry analysis of A and a replicate in the gel fluorescence experiment. (C) Blotting of total β-actin levels in SARS-CoV-2 infected and noninfected cells. (D) Densitometry analysis of relative actin levels. (E) Comparison of the signal intensity of the 25 kDa band enriched in the presence of K777 alkyne (SARS-CoV-2 infected and uninfected) versus the β-actin signal (SARS-CoV-2 infected and uninfected).

https://doi.org/10.1021/acschembio.0c00875
ACS Chem. Biol. XXXX, XXX, XXX−XXX

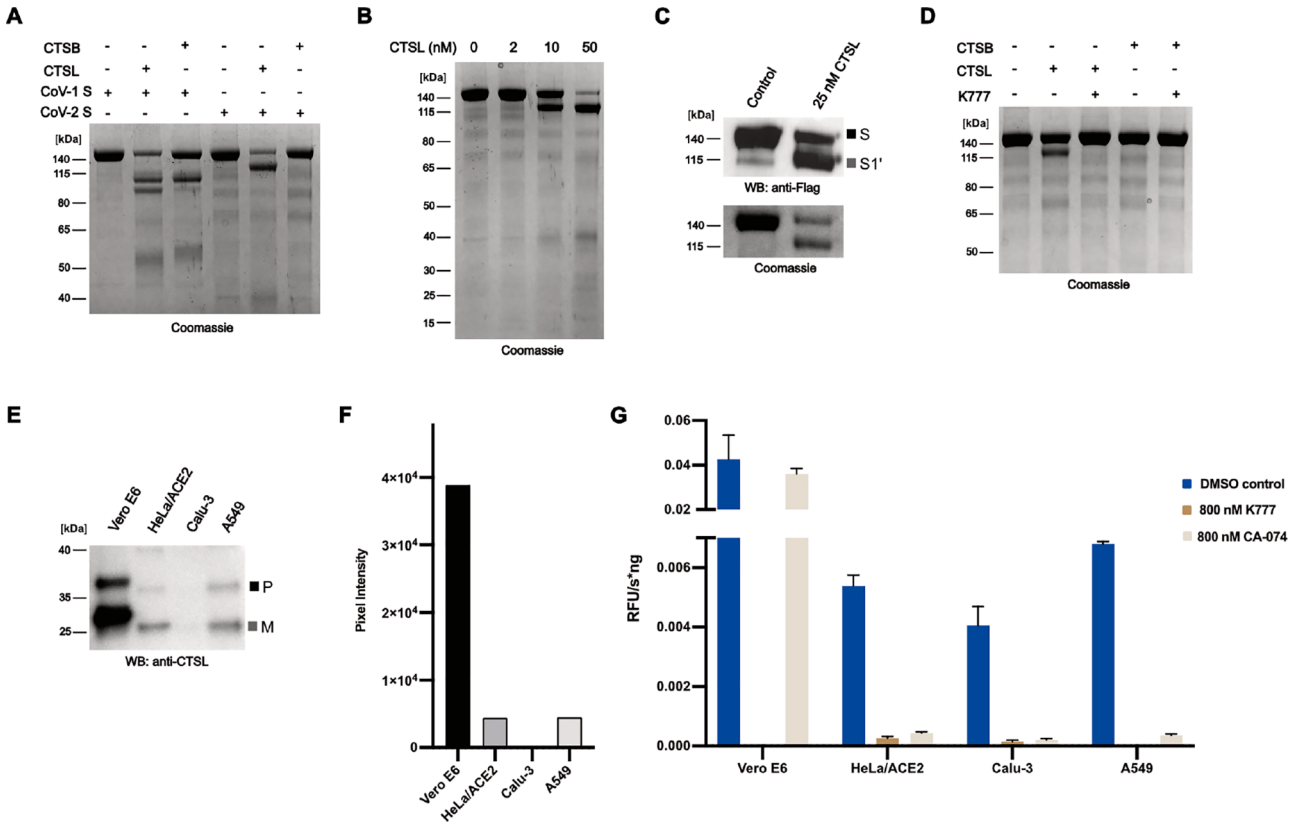

Figure 4. CTSL and CTSB catalyze differential processing of the SARS-CoV-2 spike protein, and CTSL levels vary in cells. (A) Processing of SARS-CoV-1 spike protein and SARS-CoV-2 spike protein by CTSB (250 nM) and CTSL (25 nM). (B) Concentration-dependent cleavage of the SARS-CoV-2 spike protein by CTSL. (C) Western blotting against the C-terminal FLAG epitope of SARS-CoV-2 spike demonstrates that CTSL cleavage occurs in the S1 domain. (D) CTSL (25 nM) proteolysis of the SARS-CoV-2 spike protein is inhibited by K777. (E) Western blotting against CTSL shows differential expression between cell lines (P, pro form of CTSL; M, mature form of CTSL). (F) Densitometry analysis of the mature CTSL in E. (G) Activity of cell lysates with Z-FR-AMC in the presence and absence of inhibitors.

(Figures 4A,B, S9). Additionally, processing of the SARS-CoV-2 spike protein by CSTL produced different sized molecular weight bands than that of the SARS-CoV-1 spike protein. Immunoblotting against the C-terminal Flag epitope of the SARS-CoV-2 spike resulted in immuno-reactivity with both the intact spike protein and a ∼120 kDa protein fragment, indicating that this ∼120 kDa protein contained an intact S2 domain, and that CTSL proteolysis took place in the S1 domain of the spike protein at an unknown site, which we have coined S1′ (Figure 4C). K777 efficiently blocked the cleavage at this S1′ site by CTSL of the SARS-CoV-2 spike protein (Figure 4D).

Cathepsin L Is Present in All Cell Lines Tested but Levels Vary. Although K777 targets both CTSL and CTSB, inhibition of CTSL is responsible for its potent antiviral effects. To investigate why virally infected A549/ACE2, HeLa/ACE2, and Vero E6 cells are more sensitive to K777 treatment than Calu-3 cells, we determined the relative abundance of CTSL protein in each cell line. Human CTSL shares 96% protein sequence identity with CTSL in African green monkeys (Figure S10), and therefore both the proprotein (upper band) and mature active enzyme (lower band) can be detected by immunoblot using an antihuman CTSL antibody (Figure 4E,F). Mature CTSL was 8.8-fold and 8.7-fold higher in Vero E6 extracts compared to HeLa/ACE2 and A549, respectively. Under these exposure conditions, CTSL was not detectable in Calu-3 cell extracts, consistent with a low abundance of CTSL in Calu-3 cells as has been previously described.[34,35] The large difference in CTSL abundance between these cell lines was further validated by quantitative proteomic analysis using a CTSL-derived peptide (NHCGIASSASYPTV) that is identical in humans and African green monkeys (Figure S10). This peptide was between 32- and 57-fold more abundant in Vero E6 cells compared to the other three cell lines, therefore supporting the immunoblotting studies.

Finally, we quantified the specific activity of CTSL in all four cell lines using the fluorogenic substrate Z-FR-AMC. The cell extracts were first treated with broad-spectrum serine, aspartic acid, and metallo-protease inhibitors to inactivate noncysteine proteases that may hydrolyze this substrate. The remaining activity in each cell line was eliminated by K777, confirming that only cysteine proteases were active in the non-K777 treated samples. As K777 inhibits both CTSL and CTSB, we treated the cell lines with CA-074, a selective CTSB inhibitor (Figure S12). Cysteine protease activity in A549, HeLa/ACE2, and Calu-3 cell lysates was found to be mostly due to CTSB, while activity in Vero E6 cells was mostly CTSL. The specific activity of CTSL was determined to be 0.1, 0.2, 0.5, and 36.7 RFU s^{-1} μg^{-1} for Calu-3, A549, HeLa/ACE2, and Vero E6, respectively (Figure 4G) revealing that cell lines used for the SARS-CoV-2 infection assay have high variability in CTSL abundance.

■ CONCLUSION

Three host proteases, TMPRSS-2, furin, and CTSL, have been proposed as key enzymes for the processing of the coronaviral spike protein.[16,19−21] In our analysis, we have shown that K777, a potent inhibitor of CTSL activity, is also a potent anti-SARS-

https://doi.org/10.1021/acschembio.0c00875
ACS Chem. Biol. XXXX, XXX, XXX−XXX

CoV-2 infection agent in several host cell models. Although the maximal rates of inactivation, k_{inact}, for cathepsins L, B, and K are similar, the second-order rate constant of time-dependent inactivation (k_{inact}/K_I) varies by over two orders of magnitude for these enzymes and by five orders of magnitude compared to cathepsin C, highlighting the functional selectivity of K777 for CTSL. Using a propargyl analog of K777 as an affinity probe, we determined that CTSB and CTSL were intracellular targets of this inhibitor in Vero E6 cells. However, only CTSL cleaved the SARS-CoV-2 spike protein. This cleavage occurred in the S1 domain of the spike protein at a site different from that observed in the S protein of SARS-CoV-1. The S1 domains of the spike proteins from SARS-CoV-1 and SARS-CoV-2 share 64% sequence identity, and analysis of the SARS-CoV-2 spike protein structure revealed multiple unresolved loop regions in the S1 domain, suggesting that CTSL proteolysis may occur in one of these unstructured regions.[36,37]

K777 inhibited viral entry into three host cell models including cell lines derived from African green monkey renal epithelium (Vero E6), human cervical epithelium (HeLa/ACE2), and human lung epithelium (A549/ACE2 and Calu-3/2B4) with nanomolar potency. Antiviral inhibition was lower ($EC_{50} \geq 10$ μM) in a second human lung epithelium cell line (Calu-3) lacking ACE2 receptor enhancement and a human colon epithelium-derived cell line (Caco-2; EC_{90} = 4.3 μM). Why is the efficacy of K777 different in different cell lines? On the one hand, quantification of levels of CTSL in cell lines via Western blotting and an enzyme assay confirmed that Vero E6 cells expressed the highest levels of CTSL, while HeLa/ACE2 and A549/ACE2 had lower levels. However, Calu-3 cells without ACE2 receptor enhancement had the lowest amount of CTSL protein yet were relatively insensitive to K777 treatment. This is consistent with previous reports that the cysteine protease inhibitor E64d had diminished efficacy against MERS- and SARS-CoV-2 infection of Calu-3 cells. This result was attributed to the cells containing low levels of CTSL but high levels of TMPRSS-2.[34,35] Also of note is a recent CRISPR knockout screen that identified essential host genes for SARS-CoV-2 infection. The authors suggested that TMPRSS-2, but not CTSL, was essential for viral infection of Calu-3 cells.[38] Yet, treatment of SARS-CoV-2-infected Calu-3 cells with the TMPRSS-2 inhibitor, camostat mesylate (EC_{50} = 1 μM), reduced but did not abrogate infection, leading Hoffman et al.[16] to propose that residual spike protein might require CTSL processing. In agreement with this, when using Calu-3 2B4 cells which are enriched with the spike-protein receptor ACE2, K777 was extremely potent (Table 1), suggesting this ACE2 enrichment may result in increased cathepsin L essentiality for viral penetrance.

In summary, K777 blocks primary infection of SARS-CoV-2 in several cell lines. If primary infection occurs in lung epithelium, it could be argued that the reduced ability of K777 to prevent infection of Calu-3 cells may translate into a reduced ability to prevent primary lung infections. However, the antiviral infection activity of K777 was robust in another lung epithelial cell line, A549/ACE2 (Table 1). It should also be noted that both Calu-3 and A549/ACE2 cells are derived from adenocarcinomas of the lung, not primary lung epithelium, and therefore may have multiple mutations that could alter infection potential. Recent SARS-CoV-2 patient data[39,40] indicate that levels of CTSL correlate with fatal outcomes, suggesting that CTSL may be a key protease either for infection of cells in several organs or in the inflammatory reactions that lead to severe disease.[39,40] Confirmation of these results, and the potential efficacy of dual protease inhibition,[41] will come from further tests in animal models, and ultimately in human clinical trials. Support for the rapid advancement of K777 as a potential COVID-19 therapy comes from the fact that K777 is orally bioavailable, and its safety, tolerability, and PK/PD have been evaluated in several preclinical model systems, including nonhuman primates.[30] Selva Therapeutics has been granted an open IND for K777 with the FDA (Selva Therapeutics, Del Mar, CA).

METHODS

Chemicals and Proteins. The synthesis of K777, its N-propargyl analog,[25] the 3CLpro FRET substrate, and information regarding the expression and purification of 3CLpro (Main pro) are provided in the Supporting Information. Cyanine7-azide was obtained from Click Chemistry Tools. Recombinant proteases were obtained from the following vendors: human cathepsin L (Millipore Sigma, Athens Research and Technology, Inc. (Texas A&M) or R&D Systems (UCSD)), SARS-CoV-2 PLpro (Acro Biosystems, PAE-C5184), human cathepsin S (Millipore Sigma), bovine spleen cathepsin C (Millipore Sigma), human liver cathepsin B (Millipore Sigma), and human cathepsin K (Enzo Sciences, Inc.). Substrates were purchased from the following vendors: Z-FR-AMC (EMD Millipore), GF-AMC (MP Biomedicals), and Z-LR-AMC (Enzo Life Sciences, Inc.). Recombinant SARS-CoV-1 spike protein was obtained from SinoBiological, and the SARS-CoV-2 spike protein was obtained from Genscript and Acro Biosystems.

Analysis of K777 As an Inhibitor of Clan CA Cysteine Proteases. Inhibition assays and rapid dilution assays of cathepsins B, C, K, L, and S were conducted in the presence of varied K777 (0−0.1 mM) and a fixed concentration of a dipeptide AMC substrate as described in the Supporting Information.

SARS-CoV-2 Protease Assays. Recombinant SARS-CoV-2 3CLpro was assayed at 25 °C as described in the Supporting Information using either a N-morpholino-carbonyl-(Mu)-HSSKLQ-AMC (Sigma-Aldrich, SCP0224) or FRET-based substrate Abz-SAVLQSGFRK(DNP)-NH_2 in the presence of 0−100 μM K777. Recombinant SARS-CoV-2 PL was assayed at 25 °C as described in the Supporting Information using the substrate Z-RLRGG-AMC (Bachem, I1690) in the presence of 0−100 μM K777.

Cell Cultures and SARS-CoV-2 Infection. *University of Texas Medical Branch.* African green monkey derived Vero E6 cells [CRL:1586, ATCC] were grown in Eagle's minimal essential medium (EMEM) supplemented with standard doses of penicillin and streptomycin, and 10% fetal bovine serum (FBS), designated M-10 medium. Human A549 cells stably transduced with human ACE2 viral receptor (A549/ACE2) and Calu-3 (2B4 clones selected for increased ACE2 receptor) cells were grown in M-10 and M-20 media, respectively. SARS-CoV-2 (USA_WA1/2020 isolate), the third passage in Vero E6 cells from the original CDC (Atlanta) material and sequence confirmed, was used throughout the study. All experiments using infectious virus were conducted at the University of Texas Medical Branch under BSL-3 conditions.

UC San Diego. Vero E6 cells (CRL-1586, ATCC) were cultivated in DMEM in a similar manner to that described above. Calu-3 cells (HTB-55, ATCC) were cultivated in MEM media supplemented with 10% FBS, penicillin (100 units/mL), streptomycin (100 μg/mL), and 1× GlutaMAX (Fisher Scientific). The SARS-CoV-2 virus used was the USA-WA1/2020 isolate.

Utah State University. Vero E6 cells [CRL:1587, ATCC] or Caco-2 cells [HTB-37, ATCC] were grown in minimum essential medium (MEM) containing 5% FBS or 10% FBS, respectively. The same SARS-CoV-2 (USA_WA1/2020 isolate) was used.

Evaluation of Protease Inhibitors in a Coronaviral Infection Assay. *University of Texas Medical Branch.* A modified Vero E6-based standard microneutralization assay was used to rapidly evaluate the drug efficacy against SARS-CoV-2 infection. Briefly, confluent Vero E6 or A549/ACE2 cells grown in 96-well microtiter plates were

https://doi.org/10.1021/acschembio.0c00875
ACS Chem. Biol. XXXX, XXX, XXX−XXX

pretreated with 78 nM to 25 μM K177 (2-fold serially diluted) for 2 h before infection with ∼100 or ∼500 infectious SARS-CoV-2 particles, respectively, in 100 μL of EMEM supplemented with 2% FBS (2-MEM). Cells pretreated with 2-fold serially diluted dimethyl sulfoxide (DMSO) with or without virus were included as positive and negative controls, respectively. After cultivation at 37 °C for 4 days, individual wells were observed by microscopy for the status of virus-induced formation of the cytopathic effect (CPE). The efficacy of individual drugs was calculated and expressed as the lowest concentration capable of completely preventing virus-induced CPE in 100% of the wells. Since Calu-3/2B4 cells grown in 96-well plates infected with 500 particles of SARS-CoV-2 (MO1−0.01) did not develop obvious CPEs, confluent cells grown in 24-well microtiter plates were pretreated with K777 or DMSO as described above, followed by challenge with SARS-CoV-2 at an MOI of ∼1. After 1 h of incubation, viral inoculum was removed, and cells were washed three times with 2-MEM and incubated with fresh treatments. After cultivation at 37 °C for 4 days, supernatants were harvested and titered in Vero E6 cells grown in 96-well microtiter plates using a standard infectivity assay. The titers of infectious virus were expressed as $\log_{10}$ (50% tissue culture infectious dose ($TCID_{50}$)) per milliliter.

UC San Diego. For Vero E6 and HeLa/ACE2, 1000 cells were seeded per well, and for Calu-3, 3000 cells/well. The plates were incubated for 2 h in an incubator at 37 °C and 5% CO_2. SARS-CoV-2 was added to the plate wells at a multiplicity of infection (MoI) of 1 in a final volume of 25 μL. The plates were again incubated for 24 h at 37 °C and 5% CO_2, followed by the addition of 25 μL/well of 8% paraformaldehyde solution. Cells were fixed by incubation at RT for 30 min. The content was then aspirated and the wells incubated with 1:1000 dilution of the Rabbit IgG antibody against SARS-CoV-2 capsid (Genetex, GTX135357) for 1 h and washed. Rabbit IgG coupled with AlexaFluor488 diluted 1:200 was added to the wells and incubated for at least 2 h. To calculate the antiviral activity, the average infection ratio from the untreated controls (0.1% DMSO) was normalized as 0% antiviral activity. The average infection ratio from the uninfected controls (no SARS-CoV-2) was normalized to 100% antiviral activity. A linear regression was applied to calculate the antiviral activity of each well related to the normalized controls. Serial dilution tests were performed to assess the antiviral effect and potency (IC_{50}) of K777 in the three cell lines. For the Calu-3 assay, the ATCC cell line: Calu-3 ATCC HTB-55 was used. This is a difficult cell line as cells tend to clump (see description of Calu-3/2B4 below as an alternative). Readout for the Calu-3 assay was therefore phenotypic, not based on CPE. Cells were incubated with virus in the presence of serial dilutions of K777. Immunofluorescence was used to detect the virus and to count the number of infected cells relative to nontreated (0% efficacy) and noninfected (100% efficacy) controls. There is variability in the inactive concentration as the infection ratio is variable. However, at the highest tested concentration (20 μM), K777 clearly demonstrated antiviral activity without cytotoxicity. EC_{50} values were calculated based on a curve fit model extrapolating the concentration in which the curve crossed the 50% antiviral efficacy.

Utah State University. SARS-CoV-2 CPE and virus yield reduction (VYR) assays were carried out as follows: confluent cell culture monolayers of Vero E6 or Caco-2 cells were prepared in a 96-well disposable microplate the day before testing. An insufficient CPE was observed on Caco-2 cells to use for calculation of the EC_{50} of the CPE so data were obtained after 2 h of treatment at 37 °C. CPE values were normalized based upon virus controls, and 50% effective (EC_{50}) and 50% cytotoxic (CC_{50}) concentrations were determined using nonlinear regression.

Identification of Protein Targets of K777 Using an Activity-Based Probe, K777 Alkyne. K777 alkyne (Figure 1) was added at concentrations of 1 μM to Vero E6 cells, with and without infection by SARS CoV-2 viral particles at an MoI of 0.1. For samples treated with both K777 and the K777 alkyne, Vero E6 cells were first pretreated with K777 (1 μM) for 1 h, prior to the addition of K777 alkyne (1 μM). Cell growth continued for 4 days, followed by harvest, and ∼20 million cells were suspended in 1 mL of lysis buffer (200 mM Tris, 4% CHAPS, 1 M NaCl, 8 M urea, pH 8.0) and protease inhibitor cocktail (Sigma-Aldrich, #8340) at a ratio of 50:1 (v/v). Cells were lysed by sonication (ThermoFisher); protein concentration was quantified by use of the BCA reagent (Pierce), followed by copper-mediated cycloaddition with Cy7-azide to produce covalently labeled, fluorescent proteins. K777 alkyne-labeled proteins were also covalently bound to an azide-containing bead to enrich target proteins (Click Chemistry Tools) as described in the Supporting Information, followed by SDS-PAGE separation (Invitrogen) and imaging (ChemiDoc imager, Bio-Rad).

Azide Enrichment and Proteomic Analysis of Vero E6 K777 Alkyne Treated Cells. K777 alkyne[25] was added at concentrations of 0−10 μM to Vero E6 cells. Cell lysates were prepared as described above. Enrichment of alkyne-modified proteins was conducted using the Click-&-Go Protein Enrichment Kit (Click Chemistry Tools) and the protocols therein. The resin-bound proteins were reduced with DTT, alkylated with iodoacetamide, and digested on resin using 1 μg of Trypsin Gold (Promega) at 37 °C overnight with agitation. The digested peptides were eluted from the column, desalted (Pierce C18 Tips, Thermo Fisher Scientific), concentrated to dryness, and suspended in 25 mM ammonium bicarbonate followed by nano-LC-MS/MS analysis on an Orbitrap Fusion Tribrid mass spectrometer (ThermoFisher). For more details refer to the Supporting Information.

Western Blotting. Western blotting followed a generalized protocol whereby the protein(s) of interest were transferred to a PVDF membrane, followed by blocking with TBST/nonfat milk, probing with the primary antibody of interest, washing, and the addition of the appropriate secondary antibody in TBST/nonfat milk followed by washing with TBST and chemiluminescent imaging. Detailed methods are provided in the Supporting Information.

Mammalian Protease Activity Assays. A total of 2.5 μg of SARS-CoV-1 and SARS-CoV-2 spike protein was incubated with trypsin (25 nM) in 50 mM HEPES and 1 mM Na-EDTA, at pH 7.5, or with cathepsin B (250 nM) or cathepsin L (2−250 nM) in 50 mM sodium acetate, 1 mM Na-EDTA, 1 mM CHAPS, and 1 mM DTT, at pH 5.5. Inhibitors were solubilized in DMSO and added to 10% v/v DMSO (2.5−5 μM K777 and 100 μM leupeptin). After 1 h, reactions were quenched (4× SDS-PAGE loading dye containing 5 mM DTT), denatured (95 °C, 10 min), and analyzed by SDS-PAGE (Invitrogen). Gels were either stained (Coomassie Blue) or transferred to a PVDF membrane for Western blotting as described and imaged (ChemiDoc, Bio-Rad). Protein extracts from Vero E6, HeLa/ACE2, Calu-3, and A549 cell lysates (225 ng) were incubated for 30 min with 800 nM K777 or CA-074 (Cayman #24679) in 50 mM sodium acetate (pH 5.5) containing 1 mM EDTA, 1 μM pepstatin, 100 μM AEBSF, and 5 mM DTT. These samples were then assayed with 25 μM Z-FR-AMC at 25 °C in triplicate in wells of black, flat-bottomed 384-well microplates in a total volume of 30 μL. Fluorescent activity was quantified as detailed in the Supporting Information. Selectivity of CA-074 at 800 nM was confirmed by incubating 1.1 nM recombinant human cathepsin B and cathepsin L with and without this inhibitor for 30 min and assayed with 40 μM Z-FR-AMC in a buffer consisting of 40 mM sodium acetate, at pH 5.5, 5 mM DTT, 1 mM EDTA, 100 mM NaCl, 0.001% BSA, and 1.1% DMSO. For each condition, the initial velocity in relative fluorescent units per second (RFU/s) was calculated from 10 consecutive fluorescence reads with the highest velocity within the first 30 min of the reaction.

Statistical Analysis. All densitometry was conducted using ImageJ,[42] and the calculated pixel intensities were normalized accordingly. For analysis of the statistical significance of the changes in pixel intensity, we used an unpaired parametric *t* test. *P* values ≤ 0.05 (*), ≤ 0.01 (**), and ≤ 0.001 (***).

■ ASSOCIATED CONTENT

Supporting Information

The Supporting Information is available free of charge at https://pubs.acs.org/doi/10.1021/acschembio.0c00875.

Kinetic plots, in-gel fluorescence, spike protein processing gels, additional proteomic data to identify protein targets of K777, materials, and methods (PDF)

https://doi.org/10.1021/acschembio.0c00875
ACS Chem. Biol. XXXX, XXX, XXX−XXX

AUTHOR INFORMATION

Corresponding Author

James H. McKerrow − *Skaggs School of Pharmacy and Pharmaceutical Sciences, University of California San Diego, La Jolla, California 92093, United States;* orcid.org/0000-0002-5152-4627; Email: jmckerrow@health.ucsd.edu

Authors

Drake M. Mellott − *Department of Biochemistry and Biophysics, Texas A&M University, College Station, Texas 77843, United States;* orcid.org/0000-0002-8043-8170

Chien-Te Tseng − *Department of Microbiology and Immunology, University of Texas, Medical Branch, Galveston, Texas 77755-1001, United States*

Aleksandra Drelich − *Department of Microbiology and Immunology, University of Texas, Medical Branch, Galveston, Texas 77755-1001, United States*

Pavla Fajtová − *Skaggs School of Pharmacy and Pharmaceutical Sciences, University of California San Diego, La Jolla, California 92093, United States; Institute of Organic Chemistry and Biochemistry, Academy of Sciences of the Czech Republic, 16610 Prague, Czech Republic*

Bala C. Chenna − *Department of Biochemistry and Biophysics, Texas A&M University, College Station, Texas 77843, United States;* orcid.org/0000-0002-2660-5302

Demetrios H. Kostomiris − *Department of Biochemistry and Biophysics, Texas A&M University, College Station, Texas 77843, United States*

Jason Hsu − *Department of Microbiology and Immunology, University of Texas, Medical Branch, Galveston, Texas 77755-1001, United States*

Jiyun Zhu − *Department of Biochemistry and Biophysics, Texas A&M University, College Station, Texas 77843, United States*

Zane W. Taylor − *Department of Biochemistry and Biophysics, Texas A&M University, College Station, Texas 77843, United States*

Klaudia I. Kocurek − *Department of Chemistry, Texas A&M University, College Station, Texas 77843, United States*

Vivian Tat − *Department of Microbiology and Immunology, University of Texas, Medical Branch, Galveston, Texas 77755-1001, United States*

Ardala Katzfuss − *Department of Biochemistry and Biophysics, Texas A&M University, College Station, Texas 77843, United States*

Linfeng Li − *Department of Biochemistry and Biophysics, Texas A&M University, College Station, Texas 77843, United States;* orcid.org/0000-0001-6185-4999

Miriam A. Giardini − *Skaggs School of Pharmacy and Pharmaceutical Sciences, University of California San Diego, La Jolla, California 92093, United States*

Danielle Skinner − *Skaggs School of Pharmacy and Pharmaceutical Sciences, University of California San Diego, La Jolla, California 92093, United States*

Ken Hirata − *Skaggs School of Pharmacy and Pharmaceutical Sciences, University of California San Diego, La Jolla, California 92093, United States*

Michael C. Yoon − *Skaggs School of Pharmacy and Pharmaceutical Sciences, University of California San Diego, La Jolla, California 92093, United States*

Sungjun Beck − *Skaggs School of Pharmacy and Pharmaceutical Sciences, University of California San Diego, La Jolla, California 92093, United States*

Aaron F. Carlin − *Department of Medicine, Division of Infectious Diseases and Global Public Health, University of California San Diego, La Jolla, California 92037, United States*

Alex E. Clark − *Skaggs School of Pharmacy and Pharmaceutical Sciences, University of California San Diego, La Jolla, California 92093, United States*

Laura Beretta − *Skaggs School of Pharmacy and Pharmaceutical Sciences, University of California San Diego, La Jolla, California 92093, United States*

Daniel Maneval − *Selva Therapeutics, Utah State University, Logan, Utah 84322, United States*

Vivian Hook − *Skaggs School of Pharmacy and Pharmaceutical Sciences, University of California San Diego, La Jolla, California 92093, United States;* orcid.org/0000-0001-6461-7024

Felix Frueh − *Selva Therapeutics, Utah State University, Logan, Utah 84322, United States*

Brett L. Hurst − *Institute for Antiviral Research, Department of Animal, Dairy, and Veterinary Sciences, Utah State University, Logan, Utah 84322, United States*

Hong Wang − *Institute for Antiviral Research, Department of Animal, Dairy, and Veterinary Sciences, Utah State University, Logan, Utah 84322, United States*

Frank M. Raushel − *Department of Chemistry, Texas A&M University, College Station, Texas 77843, United States;* orcid.org/0000-0002-5918-3089

Anthony J. O'Donoghue − *Skaggs School of Pharmacy and Pharmaceutical Sciences, University of California San Diego, La Jolla, California 92093, United States;* orcid.org/0000-0001-5695-0409

Jair Lage de Siqueira-Neto − *Skaggs School of Pharmacy and Pharmaceutical Sciences, University of California San Diego, La Jolla, California 92093, United States*

Thomas D. Meek − *Department of Biochemistry and Biophysics, Texas A&M University, College Station, Texas 77843, United States;* orcid.org/0000-0002-1931-8073

Complete contact information is available at: https://pubs.acs.org/10.1021/acschembio.0c00875

Author Contributions

Experimental design was provided by J.H.M., D.M.M., C.H.T., J.L.S.-N., A.D, T.D.M., F.F., A.J.O., Z.W.T., and F.M.R. These and other authors provided experimental data. The manuscript was written by J.H.M., D.M.M., C.H.T., A.J.O., J.L.N.-S., F.F, and T.D.M.

Author Contributions

[$]Thomas D. Meek and James H. McKerrow are co-senior authors.

Notes

The authors declare the following competing financial interest(s): Part of the funding for studies performed at UTMB was provided by Selva Therapeutics, Inc., and J.H.M is an advisor to Selva Therapeutics, Inc.

ACKNOWLEDGMENTS

Funding for experiments completed at Utah State University was provided by the Respiratory Diseases Branch, National Institute for Allergy and Infectious Diseases, NIH USA (Contract N01-AI-30048). Funding for the lab of T.D.M at Texas A&M was from AgriLife Research, Texas A&M University. We thank W. R. Liu (Texas A&M) for assistance

with inhibitor analysis. For the lab of C.K.T, NIAID, Grant # R24 AI120942 NPARS-S01 is acknowledged. This research was supported by a Career Award for Medical Scientists from the Burroughs Wellcome Fund to A.F.C. The following reagent was deposited by the Centers for Disease Control and Prevention and obtained through BEI Resources, NIAID, NIH: SARS-Related Coronavirus 2, Isolate USA-WA1/2020, NR-52281. Part of the funding for studies performed at UTMB was provided by Selva Therapeutics, Inc., and J.H. McKerrow is an advisor to Selva Therapeutics, Inc.

REFERENCES

(1) Zhou, P., Yang, X.-L., Wang, X.-G., Hu, B., Zhang, L., Zhang, W., Si, H.-R., Zhu, Y., Li, B., Huang, C.-L., Chen, H.-D., Chen, J., Luo, Y., Guo, H., Jiang, R.-D., Liu, M.-Q., Chen, Y., Shen, X.-R., Wang, X., Zheng, X.-S., Zhao, K., Chen, Q.-J., Deng, F., Liu, L.-L., Yan, B., Zhan, F.-X., Wang, Y.-Y., Xiao, G.-F., and Shi, Z.-L. (2020) A pneumonia outbreak associated with a new coronavirus of probable bat origin. *Nature 579*, 270−273.

(2) Morse, J. S., Lalonde, T., Xu, S., and Liu, W. R. (2020) Learning from the Past: Possible Urgent Prevention and Treatment Options for Severe Acute Respiratory Infections Caused by 2019-nCoV. *ChemBioChem 21*, 730−738.

(3) Dong, E., Du, H., and Gardner, L. (2020) An interactive web-based dashboard to track COVID-19 in real time. *Lancet Infect. Dis. 20*, 533−534.

(4) Coronavirus in the U.S.: Latest Map and Case Count. *New York Times*, 2020.

(5) Pillaiyar, T., Meenakshisundaram, S., and Manickam, M. (2020) Recent discovery and development of inhibitors targeting coronaviruses. *Drug Discovery Today 25*, 668−688.

(6) Guy, R. K., DiPaola, R. S., Romanelli, F., and Dutch, R. E. (2020) Rapid repurposing of drugs for COVID-19. *Science 368*, 829.

(7) Rota, P. A., Oberste, M. S., Monroe, S. S., Nix, W. A., Campagnoli, R., Icenogle, J. P., Peñaranda, S., Bankamp, B., Maher, K., Chen, M.-h., Tong, S., Tamin, A., Lowe, L., Frace, M., DeRisi, J. L., Chen, Q., Wang, D., Erdman, D. D., Peret, T. C. T., Burns, C., Ksiazek, T. G., Rollin, P. E., Sanchez, A., Liffick, S., Holloway, B., Limor, J., McCaustland, K., Olsen-Rasmussen, M., Fouchier, R., Günther, S., Osterhaus, A. D. M. E., Drosten, C., Pallansch, M. A., Anderson, L. J., and Bellini, W. J. (2003) Characterization of a Novel Coronavirus Associated with Severe Acute Respiratory Syndrome. *Science 300*, 1394.

(8) Zaki, A. M., van Boheemen, S., Bestebroer, T. M., Osterhaus, A. D. M. E., and Fouchier, R. A. M. (2012) Isolation of a Novel Coronavirus from a Man with Pneumonia in Saudi Arabia. *N. Engl. J. Med. 367*, 1814−1820.

(9) Zhang, L., Lin, D., Sun, X., Curth, U., Drosten, C., Sauerhering, L., Becker, S., Rox, K., and Hilgenfeld, R. (2020) Crystal structure of SARS-CoV-2 main protease provides a basis for design of improved α-ketoamide inhibitors. *Science 368*, 409.

(10) Báez-Santos, Y. M., St. John, S. E., and Mesecar, A. D. (2015) The SARS-coronavirus papain-like protease: structure, function and inhibition by designed antiviral compounds. *Antiviral Res. 115*, 21−38.

(11) Lv, L., Li, G., Chen, J., Liang, X., and Li, Y. (2020) Comparative genomic analysis revealed specific mutation pattern between human coronavirus SARS-CoV-2 and Bat-SARSr-CoV RaTG13. *bioRxiv*, No. 2020.2002.2027.969006.

(12) Heald-Sargent, T., and Gallagher, T. (2012) Ready, set, fuse! The coronavirus spike protein and acquisition of fusion competence. *Viruses 4*, 557−580.

(13) Shang, J., Wan, Y., Luo, C., Ye, G., Geng, Q., Auerbach, A., and Li, F. (2020) Cell entry mechanisms of SARS-CoV-2. *Proc. Natl. Acad. Sci. U. S. A. 117*, 11727.

(14) Ou, X., Liu, Y., Lei, X., Li, P., Mi, D., Ren, L., Guo, L., Guo, R., Chen, T., Hu, J., Xiang, Z., Mu, Z., Chen, X., Chen, J., Hu, K., Jin, Q., Wang, J., and Qian, Z. (2020) Characterization of spike glycoprotein of SARS-CoV-2 on virus entry and its immune cross-reactivity with SARS-CoV. *Nat. Commun. 11*, 1620.

(15) Belouzard, S., Chu, V. C., and Whittaker, G. R. (2009) Activation of the SARS coronavirus spike protein via sequential proteolytic cleavage at two distinct sites. *Proc. Natl. Acad. Sci. U. S. A. 106*, 5871.

(16) Hoffmann, M., Kleine-Weber, H., Schroeder, S., Krüger, N., Herrler, T., Erichsen, S., Schiergens, T. S., Herrler, G., Wu, N.-H., Nitsche, A., Müller, M. A., Drosten, C., and Pöhlmann, S. (2020) SARS-CoV-2 Cell Entry Depends on ACE2 and TMPRSS2 and Is Blocked by a Clinically Proven Protease Inhibitor. *Cell 181*, 271−280.e278.

(17) Huang, Y., Yang, C., Xu, X.-f., Xu, W., and Liu, S.-w. (2020) Structural and functional properties of SARS-CoV-2 spike protein: potential antivirus drug development for COVID-19. *Acta Pharmacol. Sin. 41*, 1141−1149.

(18) Millet, J. K., and Whittaker, G. R. (2014) Host cell entry of Middle East respiratory syndrome coronavirus after two-step, furin-mediated activation of the spike protein. *Proc. Natl. Acad. Sci. U. S. A. 111*, 15214.

(19) Zhou, Y., Vedantham, P., Lu, K., Agudelo, J., Carrion, R., Jr., Nunneley, J. W., Barnard, D., Pöhlmann, S., McKerrow, J. H., Renslo, A. R., and Simmons, G. (2015) Protease inhibitors targeting coronavirus and filovirus entry. *Antiviral Res. 116*, 76−84.

(20) Simmons, G., Gosalia, D. N., Rennekamp, A. J., Reeves, J. D., Diamond, S. L., and Bates, P. (2005) Inhibitors of cathepsin L prevent severe acute respiratory syndrome coronavirus entry. *Proc. Natl. Acad. Sci. U. S. A. 102*, 11876.

(21) Bosch, B. J., Bartelink, W., and Rottier, P. J. M. (2008) Cathepsin L Functionally Cleaves the Severe Acute Respiratory Syndrome Coronavirus Class I Fusion Protein Upstream of Rather than Adjacent to the Fusion Peptide. *J. Virol. 82*, 8887.

(22) Riva, L., Yuan, S., Yin, X., Martin-Sancho, L., Matsunaga, N., Pache, L., Burgstaller-Muehlbacher, S., De Jesus, P. D., Teriete, P., Hull, M. V., Chang, M. W., Chan, J. F.-W., Cao, J., Poon, V. K.-M., Herbert, K. M., Cheng, K., Nguyen, T.-T. H., Rubanov, A., Pu, Y., Nguyen, C., Choi, A., Rathnasinghe, R., Schotsaert, M., Miorin, L., Dejosez, M., Zwaka, T. P., Sit, K.-Y., Martinez-Sobrido, L., Liu, W.-C., White, K. M., Chapman, M. E., Lendy, E. K., Glynne, R. J., Albrecht, R., Ruppin, E., Mesecar, A. D., Johnson, J. R., Benner, C., Sun, R., Schultz, P. G., Su, A. I., García-Sastre, A., Chatterjee, A. K., Yuen, K.-Y., and Chanda, S. K. (2020) Discovery of SARS-CoV-2 antiviral drugs through large-scale compound repurposing. *Nature 586*, 113−119.

(23) Palmer, J. T., Rasnick, D., Klaus, J. L., and Bromme, D. (1995) Vinyl Sulfones as Mechanism-Based Cysteine Protease Inhibitors. *J. Med. Chem. 38*, 3193−3196.

(24) Engel, J. C., Doyle, P. S., Hsieh, I., and McKerrow, J. H. (1998) Cysteine protease inhibitors cure an experimental Trypanosoma cruzi infection. *J. Exp. Med. 188*, 725−734.

(25) Yang, P.-Y., Wang, M., He, C. Y., and Yao, S. Q. (2012) Proteomic profiling and potential cellular target identification of K11777, a clinical cysteine protease inhibitor, in Trypanosoma brucei. *Chem. Commun. 48*, 835−837.

(26) Doyle, P. S., Zhou, Y. M., Engel, J. C., and McKerrow, J. H. (2007) A Cysteine Protease Inhibitor Cures Chagas Disease in an Immunodeficient-Mouse Model of Infection. *Antimicrob. Agents Chemother. 51*, 3932.

(27) Barr, S. C., Warner, K. L., Kornreic, B. G., Piscitelli, J., Wolfe, A., Benet, L., and McKerrow, J. H. (2005) A cysteine protease inhibitor protects dogs from cardiac damage during infection by Trypanosoma cruzi. *Antimicrob. Agents Chemother. 49*, 5160−5161.

(28) Abdulla, M.-H., Lim, K.-C., Sajid, M., McKerrow, J. H., and Caffrey, C. R. (2007) Schistosomiasis Mansoni: Novel Chemotherapy Using a Cysteine Protease Inhibitor. *PLOS Medicine 4*, e14.

(29) Ndao, M., Nath-Chowdhury, M., Sajid, M., Marcus, V., Mashiyama, S. T., Sakanari, J., Chow, E., Mackey, Z., Land, K. M., Jacobson, M. P., Kalyanaraman, C., McKerrow, J. H., Arrowood, M. J., and Caffrey, C. R. (2013) A Cysteine Protease Inhibitor Rescues Mice from a Lethal Cryptosporidium parvum Infection. *Antimicrob. Agents Chemother. 57*, 6063.

(30) McKerrow, J. H. (2018) Update on drug development targeting parasite cysteine proteases. *PLoS Neglected Trop. Dis. 12*, e0005850−e0005850.

(31) Yoshikawa, T., Hill, T. E., Yoshikawa, N., Popov, V. L., Galindo, C. L., Garner, H. R., Peters, C. J., and Tseng, C.-T. (2010) Dynamic Innate Immune Responses of Human Bronchial Epithelial Cells to Severe Acute Respiratory Syndrome-Associated Coronavirus Infection. *PLoS One 5*, e8729.

(32) Thoms, M., Buschauer, R., Ameismeier, M., Koepke, L., Denk, T., Hirschenberger, M., Kratzat, H., Hayn, M., Mackens-Kiani, T., Cheng, J., Straub, J. H., Stürzel, C. M., Fröhlich, T., Berninghausen, O., Becker, T., Kirchhoff, F., Sparrer, K. M. J., and Beckmann, R. (2020) Structural basis for translational shutdown and immune evasion by the Nsp1 protein of SARS-CoV-2. *Science 369*, 1249.

(33) Cox, J., Hein, M. Y., Luber, C. A., Paron, I., Nagaraj, N., and Mann, M. (2014) Accurate proteome-wide label-free quantification by delayed normalization and maximal peptide ratio extraction, termed MaxLFQ. *Molecular & cellular proteomics: MCP 13*, 2513−2526.

(34) Park, J.-E., Li, K., Barlan, A., Fehr, A. R., Perlman, S., McCray, P. B., and Gallagher, T. (2016) Proteolytic processing of Middle East respiratory syndrome coronavirus spikes expands virus tropism. *Proc. Natl. Acad. Sci. U. S. A. 113*, 12262.

(35) Laporte, M., Stevaert, A., Raeymaekers, V., Van Berwaer, R., Martens, K., Pöhlmann, S., and Naesens, L. (2020) The SARS-CoV-2 and other human coronavirus spike proteins are fine-tuned towards temperature and proteases of the human airways. *bioRxiv*, No. 2020.2011.2009.374603.

(36) Jaimes, J. A., Millet, J. K., and Whittaker, G. R. (2020) Proteolytic Cleavage of the SARS-CoV-2 Spike Protein and the Role of the Novel S1/S2 Site. *iScience 23*, 101212.

(37) Walls, A. C., Park, Y.-J., Tortorici, M. A., Wall, A., McGuire, A. T., and Veesler, D. (2020) Structure, Function, and Antigenicity of the SARS-CoV-2 Spike Glycoprotein. *Cell 181*, 281−292.e286.

(38) Wei, J., Alfajaro, M. M., DeWeirdt, P. C., Hanna, R. E., Lu-Culligan, W. J., Cai, W. L., Strine, M. S., Zhang, S.-M., Graziano, V. R., Schmitz, C. O., Chen, J. S., Mankowski, M. C., Filler, R. B., Ravindra, N. G., Gasque, V., de Miguel, F. J., Patil, A., Chen, H., Oguntuyo, K. Y., Abriola, L., Surovtseva, Y. V., Orchard, R. C., Lee, B., Lindenbach, B. D., Politi, K., van Dijk, D., Kadoch, C., Simon, M. D., Yan, Q., Doench, J. G., and Wilen, C. B. (2021) Genome-wide CRISPR Screens Reveal Host Factors Critical for SARS-CoV-2 Infection. *Cell 184* (0020), 76−91.

(39) Zhao, M.-M., Yang, W.-L., Yang, F.-Y., Zhang, L., Huang, W., Hou, W., Fan, C., Jin, R., Feng, Y., Wang, Y., and Yang, J.-K. (2020) Cathepsin L plays a key role in SARS-CoV-2 infection in humans and humanized mice and is a promising target for new drug development. *medRxiv*, No. 2020.2010.2025.20218990, DOI: 10.1101/2020.10.25.20218990.

(40) Wu, M., Chen, Y., Xia, H., Wang, C., Tan, C. Y., Cai, X., Liu, Y., Ji, F., Xiong, P., Liu, R., Guan, Y., Duan, Y., Kuang, D., Xu, S., Cai, H., Xia, Q., Yang, D., Wang, M.-W., Chiu, I. M., Cheng, C., Ahern, P. P., Liu, L., Wang, G., Surana, N. K., Xia, T., and Kasper, D. L. (2020) Transcriptional and proteomic insights into the host response in fatal COVID-19 cases. *Proc. Natl. Acad. Sci. U. S. A. 117*, 28336.

(41) Liu, T., Luo, S., Libby, P., and Shi, G.-P. (2020) Cathepsin L-selective inhibitors: A potentially promising treatment for COVID-19 patients. *Pharmacol. Ther. 213*, 107587.

(42) Schneider, C. A., Rasband, W. S., and Eliceiri, K. W. (2012) NIH Image to ImageJ: 25 years of image analysis. *Nat. Methods 9*, 671−675.

https://doi.org/10.1021/acschembio.0c00875
ACS Chem. Biol. XXXX, XXX, XXX−XXX